13th International Symposium on Particle Image Velocimetry – ISPIV 2019
Munich, Germany, July 22-24, 2019

Pressure from Tomographic PIV: the Schur Complement method

Marco Carini[1*], Nathaniel T. Baker[1], Benjamin Leclaire[1], Franco Auteri[2]

[1] ONERA/DAAA, F-92190 Meudon, France

[2] Politecnico di Milano, Milano, Italy

[*] marco.carini@onera.fr

Abstract

This paper showcases a new method whose purpose is to reconstruct a pressure field given the full three-dimensional velocity field of an incompressible flow, acquired by tomographic PIV. This method improves the common approach based on the Poisson equation by removing the need to explicitly prescribe boundary conditions for the pressure. The main idea of the technique put forward here is to re-cast the Navier-Stokes equations into a forced Stokes problem, whose forcing term is known thanks to PIV data. In this form, the boundary conditions are naturally prescribed on the velocity field, which happens to be known everywhere inside the domain. The Stokes problem is solved thanks to a finite element approach, and the pressure is eventually obtained by solving the associated Schur complement. After giving the mathematical details of the method and of its numerical implementation, the performances of the latter are investigated on synthetic (numerical) and experimental PIV data.

1 Introduction

Thanks to the recent progress made by tomographic PIV techniques [Scarano (2012)], it is of great interest the experimental-based reconstruction of a complete pressure field throughout a spatial domain, given the non-intrusive measurement of the associated velocity field. Such measurement and reconstruction techniques offer indeed unprecedented opportunities of research, ranging from the fundamental study of turbulence and the role of the pressure-velocity correlations, to the the estimation of the loads acting on structures immersed in a flow and the investigation of aero-acoustic noise.

In order to compute a pressure field from tomo-PIV data, one must integrate the global balance of momentum for the fluid, in which the inertial and viscous terms act as a known source term. Two different approaches are usually encountered in the literature to tackle this problem [Van Oudheusden (2013), De Kat and Van Oudheusden (2012)]. The first one consists in directly integrating the pressure gradient, while the second relies on solving a Poisson equation derived by invoking the incompressible nature of the flow. Regardless of the adopted approach, it remains necessary to impose relevant boundary conditions on the pressure field in order to correctly pose the problem.

While the direct integration of the pressure gradient may theoretically be initiated from a single point in space where the pressure is known (for instance from a local measurement, or by invoking the Bernoulli equation in an irrotational part of the flow [Van Oudheusden (2008)]), such approach is known to rapidly propagate errors at each incremental step, and requires omnidirectionnal marching schemes to achieve a reliable solution [Liu and Katz (2006)]. On the other hand, solving the Poisson equation requires knowing the pressure field on the boundary of the domain, which is seldom available in an experimental context. Indeed, Pitot probes only yield punctual and intrusive measurements, while Tomo-PIV volumes are usually too small to intersect an irrotational flow everywhere. Imposing Neumann boundary conditions stemming from the global balance of momentum is neither an option, as doing so would lead to an ill-posed mathematical problem [Rempfer (2006)]. Within this context, Pan et al. (2016) showed in particular that the overall accuracy of a reconstructed pressure field is inherently linked to the type of boundary condition used (i.e. Dirichlet vs. Neumann).

As a matter of fact, in the uncoupled pressure-velocity formulation of the incompressible Navier-Stokes equations, the strict mathematical formulation of the boundary conditions associated to the Poisson equation

for pressure is of integral form [Quartapelle and Napolitano (1986)]. Dirichlet conditions for the pressure field, fully equivalent to the integral ones, can be obtained through the Glowinski-Pironneau method for pressure-velocity decoupling. [Glowinski and Pironneau (1979)]. This approach has been successfully employed by Auteri et al. (2015) for pressure reconstruction in the 2D cases. The method basically involves the solution of a set of elliptic problems as many as the total number of pressure degrees of freedom on the boundary of the domain. Therefore its extension to 3D cases, although possible, will necessarily results less computationally efficient. The method proposed here relies on the same mathematical framework introduced above while exploiting a fully discrete (or algebraic) approach for the derivation of the Poisson pressure problem, which results in a straightforward mathematical formulation and a more efficient numerical implementation for large three-dimensional PIV datasets.

The paper is structured as follows. We will start by presenting the mathematical formulation and the numerical implementation of the method in sections 2 and 3, respectively. We will then validate the algorithm on an exact analytical solution of the Navier-Stokes equations in section 4, before applying the method to synthetic and experimental PIV data in sections 5 and 6. Finally conclusions are given in section 7.

2 Principle of the method

The so-called Pressure Schur Complement (PSC) method introduced herein builds on the approach recently introduced in planar PIV by Auteri et al. (2015). Its major specificity is its discrete formulation, that leads to a simplified implementation and better computational performances. We consider the unsteady Reynolds-Averaged Navier-Stokes equations, with first-order time discretization denoted by superscripts:

$$\begin{gathered}\frac{u^n-u^{n-1}}{\Delta t}+\left(u^n\cdot\nabla\right)u^n-\nu\nabla^2u^n+\nabla p^n=-\nabla\cdot\left\langle u'^n\otimes u'^n\right\rangle \ \text{ and } \ \nabla\cdot u^n=0 \ \text{ on}\,\Omega,\\ u^n|_{\partial\Omega}=b^n,\end{gathered} \tag{1}$$

that can be recast into the following Stokes problem:

$$\begin{gathered}-\nabla^2w+\nabla\tilde{p}=g \ \text{ and } \ \nabla\cdot w=0 \ \text{ on}\,\Omega,\\ w|_{\partial\Omega}=b\end{gathered} \tag{2}$$

upon introducing the notations $\tilde{p}=p/\nu$, $w=u^n$, $b=b^n$ and $g=-\frac{1}{\nu}\left[\frac{u^n-u^{n-1}}{\Delta t}+\left(u^n\cdot\nabla\right)u^n+\nabla\cdot\left\langle u'^n\otimes u'^n\right\rangle\right]$. Right-hand side quantities of problem (2), b and g, can be computed directly from Tomo-PIV velocity fields. It is then either possible to reconstruct unsteady pressure fields from time-resolved data, upon choosing $u'^n=0$, or time-averaged pressure fields, upon setting the first term in g to zero, replacing u^n by the mean flow $\langle u\rangle$, and $\langle u'^n\otimes u'^n\rangle$ by the Reynolds stress tensor $\langle u'\otimes u'\rangle$. As specified in (2), only Dirichlet conditions on u^n or $\langle u\rangle$, directly provided by the measurements, need to be prescribed at the domain boundaries. Upon introducing a finite-element discretisation of the velocity and pressure fields, problem (2) reduces to a linear system of the form:

$$\begin{bmatrix}L_u & \tilde{G}\\ G^T & 0\end{bmatrix}\begin{pmatrix}w\\ \tilde{p}\end{pmatrix}=\begin{pmatrix}g\\ 0\end{pmatrix}. \tag{3}$$

Now, terms w, $\tilde{p}$ and g correspond to the degrees of freedom (dof) of their associated physical variables, and matrices L_u, $\tilde{G}$ and G^T to the discretized weak forms of the Laplacian, gradient and divergence operators. Note that, depending on the specific technique adopted for the implementation of Dirichlet boundary condition on the velocity, one can have $\tilde{G}^T\neq G^T$. It is then straightforward to derive a problem pertaining only to the dofs for pressure by computing the associated Schur complement, as well known in numerical methods for incompressible flows:

$$\left(G^TL_u^{-1}\tilde{G}\right)\tilde{p}=G^TL_u^{-1}g. \tag{4}$$

3 Numerical implementation

The numerical implementation of the PSC method has been performed by using the open-source finite element library FeNiCs [Logg et al. (2012)] and the open-source library of linear algebraic solvers PETSc

[Balay et al. (2018)]. The Stokes system (2) has been discretised on an unstructured tetrahedric mesh (directly obtained from the original PIV Cartesian mesh) by using a classical Taylor-Hood P2-P1 formulation, thus fully satisfying the well-known *inf-sup* condition associated with the incompressibility constraint. While the sparse matrices L_u, $\tilde{G}$ and G^T are thus assembled, the explicit construction and storage of the PSC matrix $G^T L_u^{-1} \tilde{G}$ is never performed due to its dense structure. Instead, the Schur linear system is solved by an iterative approach, through the GMRES algorithm available within PETSc, thus only requiring matrix-vector multiplications to be performed. The same algorithm, with an additional algebraic multigrid preconditionner, has also been employed for the efficient numerical inversion of the large-scale matrix L_u, as required at each iteration of the external PSC GMRES loop. Therefore a two-level nested GMRES approach is used to solve (4). Both the finite element assemblage and the inversion of the involved large-scale matrices have been performed in parallel thanks to the inherent parallelism of the employed numerical libraries and the available ONERA HPC facilities.

4 Validation and performance assessment on an analytical solution

The PSC method and its convergence properties are here validated with respect to an analytical solution. For this purpose, we consider the following pressure field mimicking a vortical flow:

$$p_{\text{ref}} = \rho U_0^2 \left[-\frac{1}{8} \sin^2(x) \left(\sin^2(y) + \sin^2(z) \right) + \frac{1}{4} \sin^2(y) \sin^2(z) \right] e^{-6\nu t}. \tag{5}$$

The above pressure field is an exact solution to the unsteady Navier-Stokes equations subject to the external forcing $\vec{f}$

$$\frac{\partial \vec{u}}{\partial t} + \vec{u} \cdot \nabla \vec{u} = -\frac{\nabla p}{\rho} + \nu \Delta \vec{u} + \frac{\vec{f}}{\rho}, \tag{6}$$

with

$$\vec{u} = U_0 \begin{pmatrix} -\cos(x)\sin(y)\sin(z) \\ \frac{1}{2}\sin(x)\cos(y)\sin(z) \\ \frac{1}{2}\sin(x)\sin(y)\cos(z) \end{pmatrix} e^{-3\nu t}, \tag{7}$$

and

$$\vec{f} = -\frac{3}{4} \rho U_0^2 \begin{pmatrix} \cos(x)\sin(x)\left(\sin^2(y) + \sin^2(z)\right) \\ 0 \\ 0 \end{pmatrix} e^{-6\nu t}. \tag{8}$$

Figure 1 shows the magnitude of the velocity field (left) and the pressure field (right) given before. These fields are sampled across a three-dimensional cubic domain of size $L = 2\pi$, with $N = 32$ points in each spatial direction.

4.1 Sensitivity to spatial resolution

First of all, let us assess the convergence of the reconstructed pressure field with respect to the spatial resolution $h = L/N$, where N represents the number of points used to discretise the domain along each spatial direction. The relative error between the exact solution p_{ref} (Eq. 5) and the pressure p numerically reconstructed using the Schur complement method fed with the velocity field $\vec{u}$ (Eq. 7) is quantified using both the classical ℓ_2 and ℓ_∞ norms for the nodal pressure values, respectively defined by

$$E_2 = \sqrt{\frac{\sum_\Omega (p_{\text{ref}} - p)^2}{\sum_\Omega p_{\text{ref}}^2}}, \tag{9}$$

and

$$E_\infty = \frac{\max |p_{\text{ref}} - p|}{\max |p_{\text{ref}}|}. \tag{10}$$

Results are reported in figure 2, clearly confirming that the pressure field reconstructed using the PSC method converges towards the exact solution p_{ref} with second-order spatial accuracy, as expected.

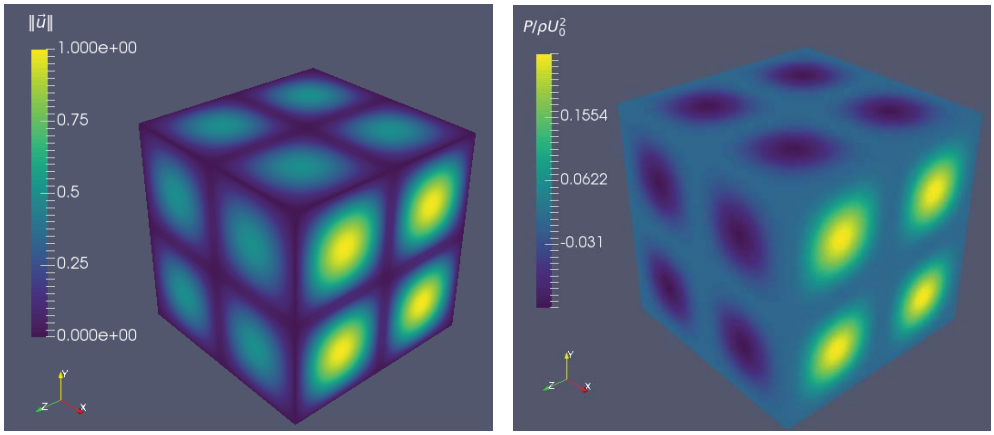

Figure 1: (Left) Visualization of the velocity field $\vec{u}$ given by Eq. 7. (Right) Reference pressure field given by Eq. 5

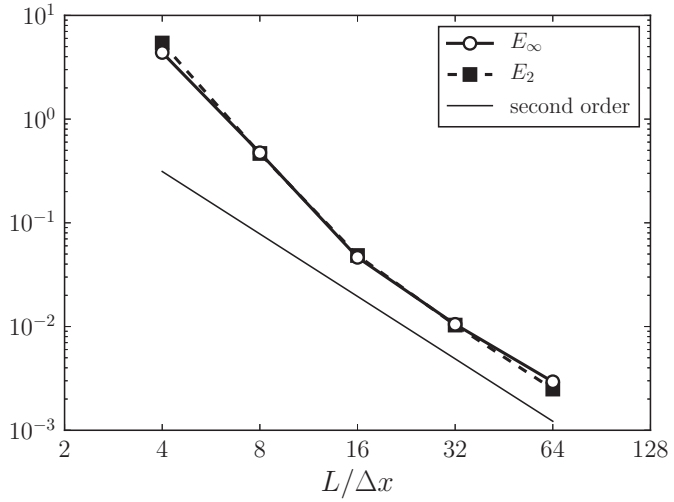

Figure 2: Convergence behavior of the Schur complement method with respect to spatial resolution.

4.2 Sensitivity to noise

Since experimental data is inherently corrupted by some level of noise, the robustness of the algorithm to the presence of the noise is here briefly investigated. The adopted methodology consists in adding a random noise with a Gaussian distribution to each component of the input velocity field, and at each vertex in the computational domain. The noise is assumed to be spatially uncorrelated, but time correlated (indeed assuming a white noise also in time will lead to very large errors when computing its derivative). The noise level is characterized by the standard deviation σ, with $\sigma = 1, 5$ and 10% of U_0.

Figure 3 displays the pressure mean error distribution (left) and the standard deviation distribution (right) over the entire domain. These statistics have been computed over 500 trials, which yield a convergence level better than 10^{-4}. This figure shows that the spatial distribution of the mean error is not uniform throughout space. On the one hand, comparing the spatial distribution of the mean error on the reconstructed field with the velocity field (Figure 1) suggests that the mean error is maximum where the velocity gradient is maximum. On the other hand, comparing the spatial distribution of the error's standard deviation suggests that it scales as the amplitude of the velocity field, in contrast to what observed by Auteri et al. (2015).

A more quantitative description of the impact of noise on the results is shown in Figure 4, which displays the statistical distribution of the error on the pressure field (ε_P). As a reference, the noise distribution added to all three velocity components is shown (ε_U, ε_V, ε_W), which confirms that it is indeed Gaussian. Interestingly,

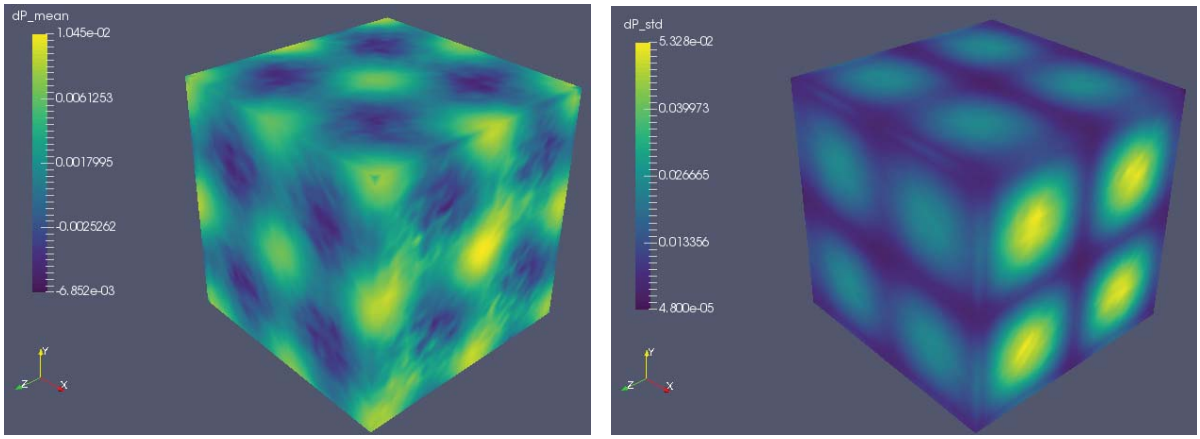

Figure 3: (Left) Spatial distribution of the mean error. (Right) Spatial distribution of the error standard deviation.

the error distribution of the reconstructed pressure dramatically departs from a Gaussian distribution, and is much flatter than the latter. This means that the expected errors made on the reconstructed pressure field are larger than those on the velocity. Yet, the amplitude of the error on the reconstructed pressure still scales according to the amplitude of the noise added to the velocity field.

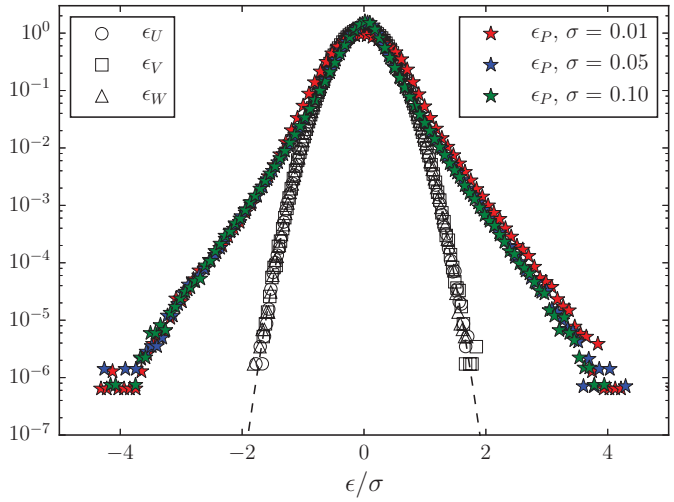

Figure 4: Probability distribution of the error on the reconstructed pressure p (colored symbols) for a Gaussian distribution of the error on the velocity field (empty symbols, one for each spatial coordinate).

5 Demonstration on synthetic PIV data

Let us now apply the method to synthetic PIV data numerically generated by an IDDES simulation performed by Gomit et al. (2018). The geometry adopted here is a NACA0015 wing of 80 mm chord and 140 mm span, placed at a 30^o angle of attack in a 230 mm $\times$ 230 mm square hydraulic tunnel. The free-stream value of the incoming flow is fixed at $U = 1.25\,\mathrm{m/s}$, which corresponds to a Reynolds number based on the chord of $Re_c = 100,000$. The computed flow is then extracted along three sub-volumes of the computational domain,which mimic typical Tomo-PIV volumes (cf. Figure 5). The data within these volumes has been filtered to simulate the smoothing effect of PIV, and the resulting spatial resolution is 1 mm.

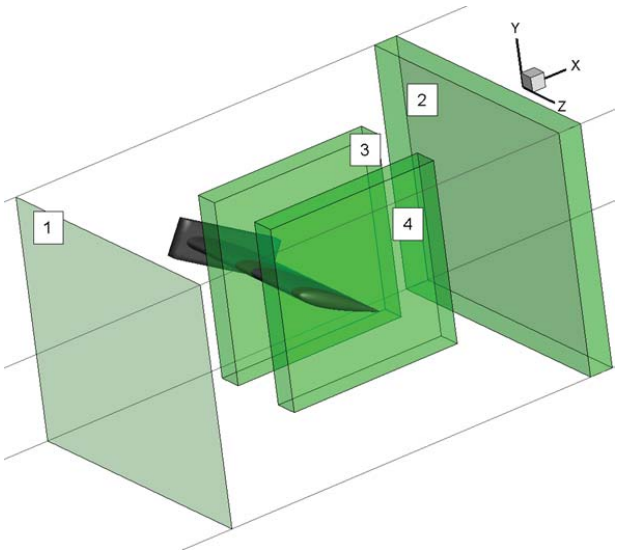

Figure 5: Visualization of the PIV volumes extracted from the numerical database.

The pressure field was reconstructed in volumes 2 and 4 of figure 5. Doing so makes it possible to assess the behavior of the method in two different situations: in the wake of an airfoil (volume 2), and in the presence of a rigid obstacle (volume 4). The pressure reconstruction was performed on one of ONERA's clusters. The most computational intensive case (i.e. the wake in volume 4) required to solve a linear system of size 689778×689778 for the pressure and 15843927×15843927 for the velocity, whose convergence was reached in 83 GMRES iterations. As a matter of fact, the computation took about 20 minutes, thanks to the parallelization of the job on 250 processors. The maximum memory required during the job was 152 Gb.

Figure 6 provides 2D views of the reconstructed pressure field along the mid-plane of volumes 4 and 2 respectively. The top graphs show the actual pressure field, while the bottom graphs give the relative error between the reconstructed pressure field and the reference pressure field given by the simulation. Note that these plots use log colorbars. As with the analytical case studied earlier, this figure confirms that the error distribution is not uniform throughout the PIV domain, and is strongly linked to the presence of velocity gradients. Indeed, the error appears to be highest at the location of rigid obstacles where the no-slip boundary condition applies, and in the presence of strong vortical structures. A global estimate for the accuracy of the reconstructed pressure using the ℓ_2 norm (Eq. 9) yields $E_2 = 10\%$ in volume 2 and $E_2 = 3\%$ in volume 4.

6 Demonstration on experimental data

To assess the method's performance in real conditions, the flow around a generic flying wing model (SACCON configuration, see e.g. Schütte et al., 2012), at a chord Reynolds number of 1.1×10^6 and angle-of-attack of 20^o, has been considered. Tomographic PIV experiments have been performed in ONERA L1 wind-tunnel of the Lille ONERA centre. A sketch of the model and a picture of the experimental setup are reported in Figure 7. The volume illumination has been placed so as to capture the wingtip vortex, and to match with a generatrix of pressure taps located on the wing surface, yielding a reference for the reconstruction. Further details and results are described in our companion paper by Baker et al.

Volumic mean pressure computation using the PSC method in RANS mode has been performed using mean flows and Reynolds stresses resulting from tomographic PIV. In practice, for the case presented here, this led to solve a 58378737×58378737 system, which was run on 840 cores, and required up to 1.05 TB of memory. Figure 8 shows results of this reconstruction in the plane coinciding with the pressure tap generatrix at the model wall. Quantity displayed are contours of pressure coefficient $C_p = 2(p - p_\infty)/\rho U_\infty$ in the whole plane, and extracted closest to the wall for comparison with the taps. In the case of PSC, no particular tap was used as a reference for the absolute pressure level. Instead, it was preferred to choose this reference value so that the integral of both C_p curves (PSC and pressure taps) coincide, in order not to favor a particular

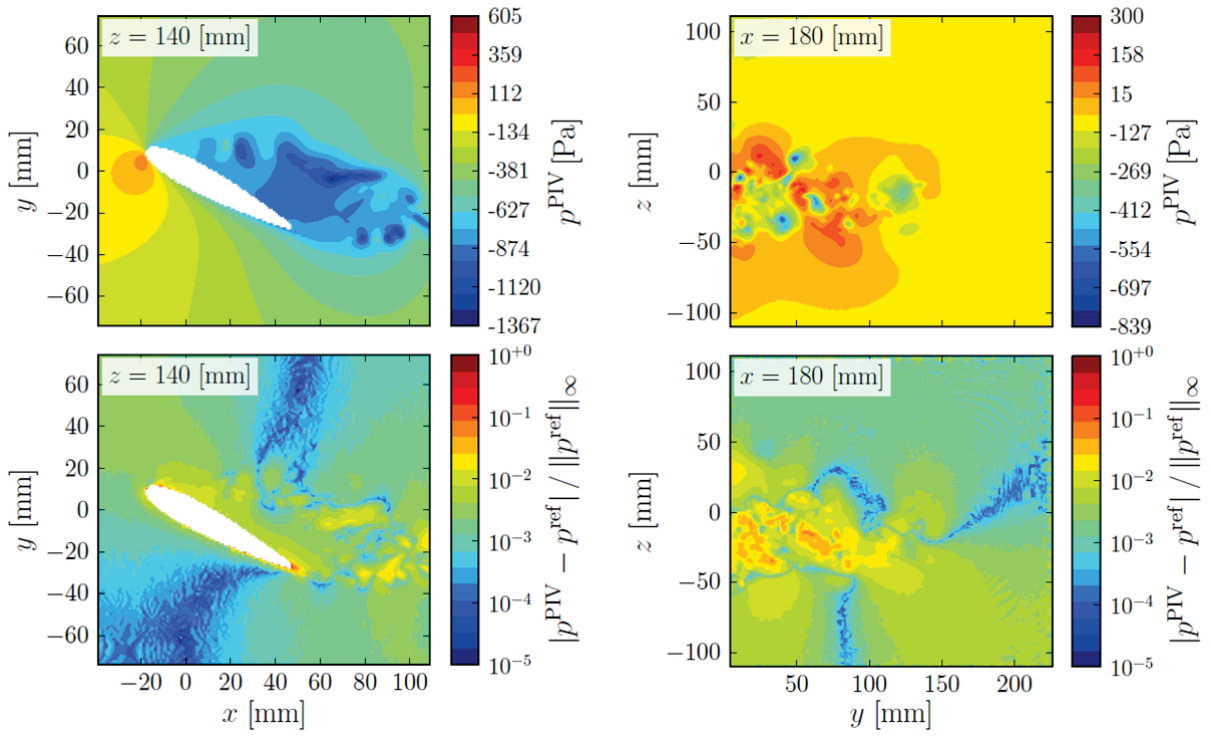

Figure 6: Performance assessment on two volumes extracted from an IDDES numerical simulation around a finite span NACA0015 wing ($Re_c = 100,000$, see Gomit et al., 2018). Top: Reconstructed pressure fields. Bottom: Relative error between reconstruction and ground truth (note the use of a log scale). Left column corresponds to a flow zone close to the wingtip, right column to a zone within the wing wake.

sensor. As seen in Figure 8, the PSC method appears to capture truthfully the signature of the leading edge vortex, which is characterized by a strong depression at the location of the vortex core. The pressure profile extracted closest to the wing's upper surface compares well with the pressure tap measurements (cf. Figure 8, right) along almost the whole profile, for $-0.16 \leq y \leq -0.10$. For $y \geq -0.8$, i.e. closest to the vortex core, reconstructed C_p however deviates from the pressure tap measurements. This is probably to be ascribed to the fact that, due to remaining light reflection, the lower edge of the reconstructed volume does not exactly coincide with the wall, but is rather located a few mm above. As it is well known, curved streamlines (such as in the case of a vortex) are associated with a pressure gradient normal to the curvature, so that extrapolation of pressure directly below a vortex core can be particularly error-prone.

7 Conclusion

This paper has presented a new method to reconstruct a pressure field from the tomo-PIV measurements of an incompressible flow. This method essentially relies on re-casting the Navier-Stokes equations into a forced Stokes problem, whose forcing term is completely determined by experimental data. Under this form, boundary conditions have to be prescribed only for the velocity field (which is known everywhere from the PIV measurements) by contrast to other Poisson-based approaches available in the literature, requiring explicit pressure boundary data which are rarely accessible experimentally.

First, the soundness of the algorithm has been validated against an analytical solution of the unsteady incompressible Navier-Stokes equations in order to assess the convergence of the method with respect to spatial, as well as its filtering behaviour w.r.t. to spatial noise. In particular, we have shown that the amplification of noise in the velocity data (which is unvoidable experimentally) roughly scales according to the amplitude of the noise on the velocity field.

We have then assessed the quality of the reconstructed pressure field on a more realistic application, namely a time-resolved numerical simulation of the flow around a NACA0015 airfoil, and a time-averaged

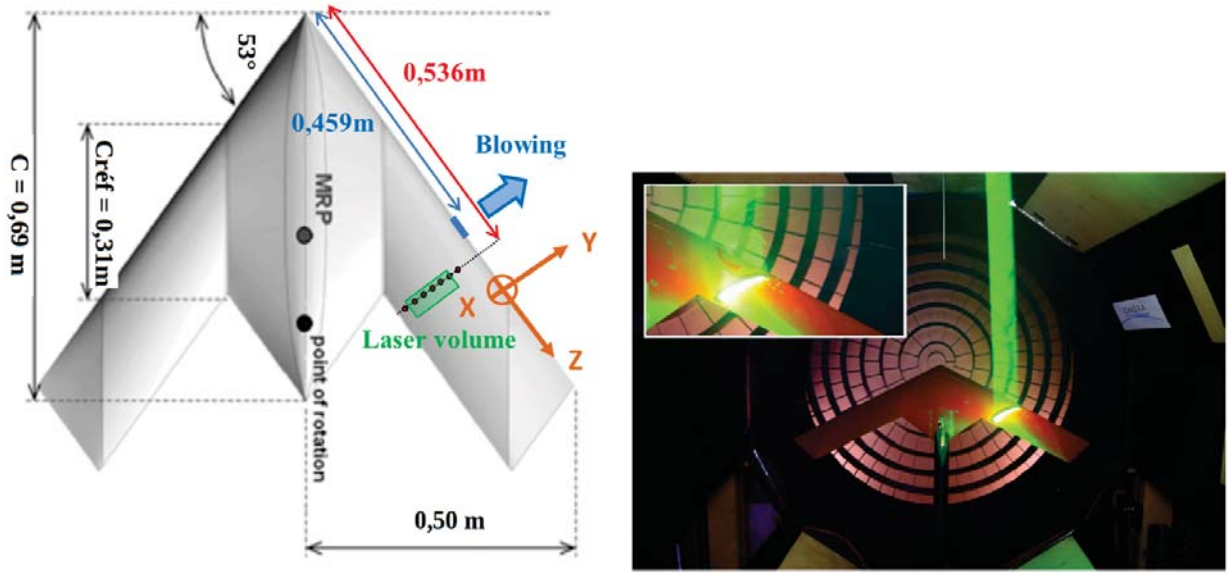

Figure 7: SACCON Experimental: sketch of the flying wing model for PIV measurement (left); picture of the PIV experimental setup (right).

actual experiment of the flow over the upper surface of a flying wing. As observed for the analytical solution, the error on the reconstructed pressure in the complex flow around the airfoil is not uniform and strongly depends on the flow gradients as encountered approaching the walls and in the core region of vortical structures.

Last but not least, the promising results obtained for the SACCON flying wing configuration have proved that the method is indeed applicable even to industrial-size facilities, which paves the way for advanced applications in the aerospace industry.

Acknowledgements

The authors acknowledge the financial support of the Agence National pour la Recherche and the DGA under the grant ANR-16-ASTR-0005-01, as well as the CPER-FEDER of the Hauts-de-France and Nouvelle-Aquitaine regions.

References

Auteri F, Carini M, Zagaglia D, Montagnani D, Gibertini G, Merz CB, and Zanotti A (2015) A novel approach for reconstructing pressure from piv velocity measurements. *Exp Fluids* 56:45

Balay S, Abhyankar S, Adams MF, Brown J, Brune P, Buschelman K, Dalcin L, Eijkhout V, Gropp WD, Kaushik D, Knepley MG, May DA, McInnes LC, Mills RT, Munson T, Rupp K, Sanan P, Smith BF, Zampini S, and Zhang H (2018) PETSc Web page: http://www.mcs.anl.gov/petsc

De Kat R and Van Oudheusden BW (2012) Instantaneous planar pressure determination from piv in turbulent flow. *Exp Fluids* 52:1089–1106

Glowinski R and Pironneau O (1979) On a mixed finite element approximation of the stokes problem (i). *Num Math* 33:397–424

Gomit G, Carini M, Dartois A, Baker N, Beaudoin A, Leclaire B, Pons F, Chatellier L, Tremblais L, Lionel T, Braud P, and David L (2018) Comparaison de méthodes dévaluation de la pression partir de mesures piv. *16ème Congrès Francophone de Techniques Laser*

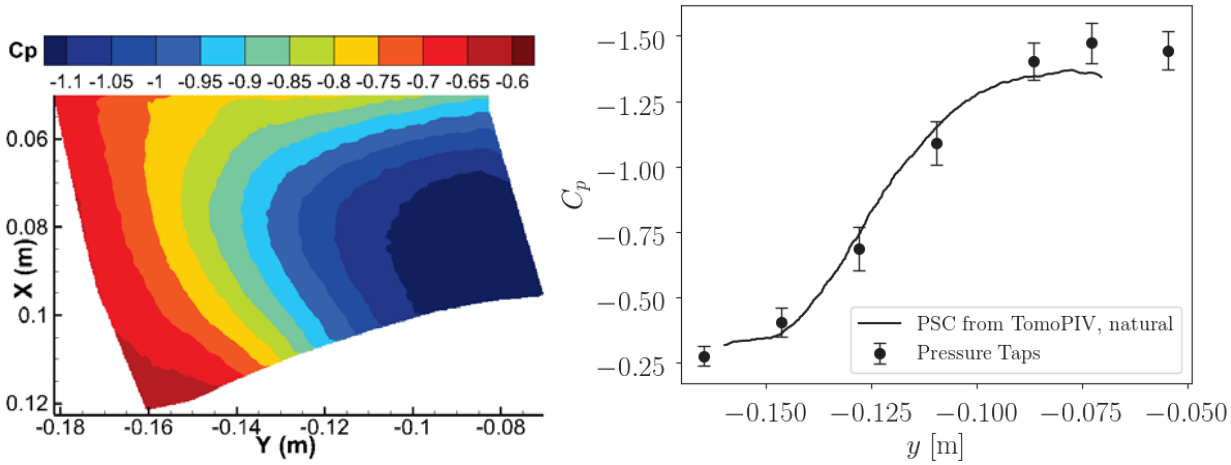

Figure 8: Results of PSC pressure reconstruction from Tomo PIV measurements of the SACCON test case. Left: C_p contours in the plane containing pressure taps. Right: Comparison between the pressure taps and reconstructed pressure extracted along the line at the bottom edge of the domain.

Liu X and Katz J (2006) Instantaneous pressure and material acceleration measurements using a four-exposure piv system. *Exp Fluids* 41:227

Logg A, Mardal KA, Wells GN et al. (2012) *Automated Solution of Differential Equations by the Finite Element Method*. Springer

Pan Z, Whitehead J, Thomson S, and Truscott T (2016) Error propagation dynamics of piv-based pressure field calculations: How well does the pressure poisson solver perform inherently?. *Meas Science Technol* 27:084012

Quartapelle L and Napolitano M (1986) Integral conditions for the pressure in the computation of incompressible viscous flows. *J Comp Phys* 62:340–348

Rempfer D (2006) On boundary conditions for incompressible navier-stokes problems. *App Mech Rev* 59:107–125

Scarano F (2012) Tomographic piv: principles and practice. *Meas Science Technol* 24:012001

Schütte A, Hummel D, and Hitzel SM (2012) Flow physics analyses of a generic unmanned combat aerial vehicle configuration. *Journal of Aircraft* 49:1638–1651

Van Oudheusden BW (2008) Principles and application of velocimetry-based planar pressure imaging in compressible flows with shocks. *Exp Fluids* 45:657–674

Van Oudheusden BW (2013) Piv-based pressure measurement. *Meas Science Technol* 24:032001